

# Energy balance of optical breakdown in water at nanosecond to femtosecond time scales

A. Vogel<sup>1,\*</sup>, J. Noack<sup>1</sup>, K. Nahen<sup>1</sup>, D. Theisen<sup>1</sup>, S. Busch<sup>1</sup>, U. Parlitz<sup>2</sup>, D.X. Hammer<sup>3</sup>, G.D. Noojin<sup>3</sup>, B.A. Rockwell<sup>3</sup>, R. Birngruber<sup>1</sup>

<sup>1</sup>Medizinisches Laserzentrum Lübeck, Peter-Monnik Weg 4, D-23562 Lübeck, Germany  
(Fax: +49-451/505-486, E-mail: vogel@mll.mu-luebeck.de)

<sup>2</sup>Drittes Physikalisches Institut, University of Göttingen, Bürgerstr. 42-44, D-37073, Germany  
(Fax: +49-551/397-720, E-mail: ulli@physik3.gwdg.de)

<sup>3</sup>Airforce Research Laboratory, Brooks AFB, TX 78235, USA  
(Fax: +1-210/536-3903, E-mail: ben.rockwell@hedo.brooks.af.mil)

Received: 3 August 1998/Revised version: 20 October 1998

**Abstract.** During optical breakdown, the energy delivered to the sample is either transmitted, reflected, scattered, or absorbed. Pathways for the division of the absorbed energy are the evaporation of the focal volume, the plasma radiation, and the mechanical effects such as shock wave emission and cavitation. The partition of laser energy between these channels during breakdown in water was investigated for four selected laser parameters typical for intraocular microsurgery (6-ns pulses of 1 and 10 mJ focused at an angle of 22°, and 30-ps pulses of 50  $\mu$ J and 1 mJ focused at 14°, all at 1064 nm). Scattering and reflection were found to be small compared to transmission and absorption during optical breakdown. The ratio of the shock wave energy and cavitation bubble energy was approximately constant (between 1.5:1 and 2:1). These results allowed us to perform a more comprehensive study of the influence of pulse duration (100 fs–76 ns) and focusing angle (4°–32°) on the energy partition by measuring only the plasma transmission and the cavitation bubble energy. The bubble energy was used as an indicator for the total amount of mechanical energy. We found that the absorption at the breakdown site first decreases strongly with decreasing pulse duration, but increases again for  $\tau < 3$  ps. The conversion of the absorbed energy into mechanical energy is  $\approx 90\%$  with ns pulses at large focusing angles. It decreases both with decreasing focusing angle and pulse duration (to  $< 15\%$  for fs pulses). The disruptive character of plasma-mediated laser effects is therefore strongly reduced when ultrashort laser pulses are used.

**PACS:** 62.50.+p; 79.20.Ds; 87.00

Nonlinear absorption through laser-induced breakdown [1, 2] can occur at material surfaces as well as inside media which are transparent at low light intensities. As a tool for surface

ablation, optical breakdown competes with material ablation based on linear absorption [3–5]. Optical breakdown *inside* of linearly transparent media, on the other hand, offers a possibility of localized energy deposition which can be achieved by no other optical means. This unique feature enables non-invasive surgery inside the eye [1, 6], and it has been suggested to apply it for the design of 3-dimensional storage elements [7].

The advent of compact and reliable ultrashort pulse lasers has made it possible to achieve very fine laser effects, because the energy threshold for optical breakdown decreases with a reduction of pulse duration [8, 9]. Besides on the breakdown threshold, the laser effects also depend on the partition of the incident energy in various pathways. Only the absorbed energy is effective for material processing; light transmission through the plasma as well as scattering and reflection by the plasma reduce the efficacy of the plasma-mediated process. Absorbed energy going into evaporation contributes to the tissue cutting or material ablation, whereas the energy going into the mechanical pathways of shock wave generation and cavitation contributes to the disruptive character of the breakdown process [10, 11]. The latter may be advantageous in some cases (for example in posterior capsulotomy [12] and lithotripsy [1]), but it is often a source of unwanted side effects. Knowledge of the energy partition during optical breakdown is thus a prerequisite for an optimal parameter choice for each particular application.

In this paper we establish, for the first time, a complete energy balance of optical breakdown in water. Detailed results are presented for selected laser parameters typical for intraocular microsurgery, and the dependence of energy partition on the focusing angle  $\theta$  and on laser pulse duration  $\tau_L$  is analyzed for a large parameter range ( $4^\circ < \theta < 32^\circ$ ,  $100 \text{ fs} < \tau_L < 76 \text{ ns}$ ).

We used distilled water as a model substance for the transparent media of the eye. This simplification guaranteed reproducibility of the experimental results and is justified by

\* To whom all correspondence should be addressed

the fact that the thresholds for optical breakdown in distilled water are very similar to the breakdown thresholds in ocular media [13, 14]. Similarities are also found between the mechanical properties of water and those of aqueous humor and the vitreous substance, whereas they are different for the lens and cornea. The different mechanical properties of lens and cornea result mainly in changes of the bubble dynamics; the shock wave emission is much less affected, because the acoustic impedances are similar for water and tissue. The differences in bubble dynamics are probably not very pronounced during the initial phase of the bubble expansion when the plastic flow stress of the tissue is exceeded, but become stronger during later times when the elastic properties of the tissue lead to a limitation of the maximum bubble size. It is, however, during the initial phase after breakdown when the energy partition into the different mechanical and non-mechanical pathways occurs. The similarity of this phase for water and tissue suggests that the results of our investigations on water should also be applicable for various types of transparent tissues.

## 1 Methods

### 1.1 Optical system for plasma generation

Optical breakdown was produced by focusing laser pulses with various durations between 76 ns and 100 fs into a cuvette containing distilled water (Fig. 1). The optical delivery system allowed for the realization of different focusing angles and was designed to minimize spherical aberrations. For that purpose, an ophthalmic contact lens was built into the cuvette wall. A detailed description of the optical system for plasma generation and of the methods used for the measurement of the focusing angle, the spot size, and the optical breakdown threshold has been given previously [8, 11, 15]. The laser parameters used together with the respective spot sizes and breakdown thresholds are summarized in Table 1.

### 1.2 Plasma transmission, scattering and reflection

The plasma transmission  $T$  was measured with the setup depicted in Fig. 1a [16]. For each focusing angle  $\theta$  of the

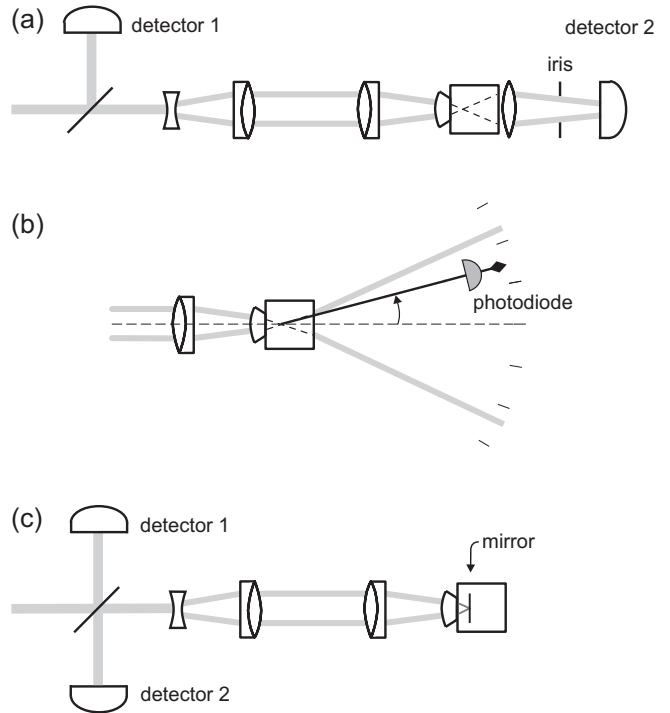


**Fig. 1a–c.** Setup for the measurement of plasma transmission (a), forward scattering (b), and back reflection into the focusing optics (c)

incident light, only light transmitted within that angle was collected; light scattered out of the cone angle of the laser beam was rejected by an iris diaphragm. To account for light losses by reflections at optical surfaces and water absorption, detector 2 was calibrated against detector 1 assuming that at pulse energies far below breakdown threshold 100% of the incident energy is transmitted through the laser focus.

The amount of light scattered out of the cone angle of the laser beam was determined through goniometric measurements performed in steps of  $2^\circ$  for  $\alpha \leq 10^\circ$  and in steps of  $5^\circ$  for  $10^\circ \leq \alpha \leq 45^\circ$  [16] (Fig. 1b). To assess the amount of forward scattering  $S$  by the plasma, we compared the angular energy distribution at a given superthreshold energy  $\beta = E/E_{th}$  to the distribution it has below threshold. The measurement technique was described in detail in a previous paper [16].

**Table 1.** Laser parameters investigated in the present study, and corresponding spot sizes and breakdown thresholds. A complete energy balance was established for 6-ns pulses at  $22^\circ$  (1 and 10 mJ pulse energy) and 30-ps pulses at  $14^\circ$  (50  $\mu$ J and 1 mJ pulse energy). The dependence of energy partition on focusing angle was investigated for 6-ns and 30-ps pulses. The dependence on pulse duration was investigated for 76-ns pulses, 6-ns pulses at  $22^\circ$ , 60 ps, 3 ps, 300 fs, and 100 fs

Pulse duration	Wavelength nm	Focusing angle $^\circ$	Measured spot diameter / $\mu$ m	$I_{th}$ $\times 10^{11}$ W cm $^{-2}$	$F_{th}$ J cm $^{-2}$
76 ns	750	19	20	0.23	1750
6 ns	1064	32	5.5	0.66	398
6 ns	1064	22	7.6	0.47	284
6 ns	1064	8	11.5	0.79	472
6 ns	1064	5.4	14.6	1.1	648
30 ps	1064	28	4.6	4.6	13.8
30 ps	1064	22	4.7	4.5	13.6
30 ps	1064	14	5.8	3.0	9.0
30 ps	1064	8.5	9.6	4.5	13.6
30 ps	1064	4	19.5	3.7	11.1
60 ps	532	13	5.6	2.8	16.8
3 ps	580	16	5.0	8.5	2.6
300 fs	580	16	5.0	47.6	1.4
100 fs	580	16	4.4	111.0	1.1

The amount of light reflected by the plasma back into the cone angle of the focused laser beam was measured using the setup in Fig. 1c [16]. First, an aluminum mirror was placed into the focus and a measurement was performed at an energy where no plasma formation on the mirror occurred. In this way the calibration factor between the two detectors was determined for a case with a known reflection of 80%. The mirror was then removed and the plasma reflection  $R$  measured at higher pulse energies.

Direct investigation of the energy absorbed in the breakdown volume would require measurements with a water-filled integrating sphere. At a wavelength of 1064 nm where the absorption coefficient of water is  $0.13 \text{ cm}^{-1}$ , such measurements are, however, difficult, because no equilibrium light distribution can be achieved within the sphere. We therefore deduce the absorption  $A$  from the measurements of transmission, scattering, and reflection:  $A = (1 - T - S - R)$ .

### 1.3 Evaporation energy

To assess the evaporation energy, we assume that the water within the plasma volume is completely evaporated, but neglect any enlargement of the evaporated liquid volume by heat conduction. The influence of heat conduction can be neglected in a first approximation, because the laser pulse duration is extremely short ( $\leq 6 \text{ ns}$ ), and the content of the cavitation bubble produced by the expansion of the hot plasma cools down to room temperature within a few  $\mu\text{s}$  [17]. The penetration depth  $\delta$  of heat diffusion is given by [18]:

$$\delta = (4\kappa\tau_R)^{1/2}, \quad (1)$$

where  $\tau_R$  is the thermal relaxation time and  $\kappa = 0.15 \text{ mm}^2/\text{s}$  is the thermal diffusivity of water at  $37^\circ$  [19]. For a thermal relaxation time of a few  $\mu\text{s}$ ,  $\delta$  is in the order of  $1\text{--}2 \mu\text{m}$  which is small compared to the plasma size observed at the laser parameters investigated. The plasma volume  $V_p$  was determined from photographs of the plasma luminescence [8].

We use the isobaric evaporation enthalpy and specific heat to account for the amount of energy consumed for the vaporization of  $V_p$ . Immediately after the laser pulse, pressure and temperature in the breakdown volume are very high and the liquid is in a supercritical state. At this point in time, mechanical energy and evaporation energy are not yet separable. After a small fraction of the cavitation bubble lifetime, however, the pressure has decayed to values close to the hydrostatic pressure, the mechanical energy leading to cavitation bubble formation and shock wave emission has been imparted to the liquid surrounding the breakdown volume, and the heated material within the breakdown volume has changed into the vapor state. The energy required for the heated material to be transformed into vapor of  $100^\circ\text{C}$  is given by

$$E_V = \rho_0 V_p [c(T_2 - T_1) + r], \quad (2)$$

with  $\rho_0 = 998 \text{ kg m}^{-3}$ ,  $c = 4.18 \text{ kJ (kg K)}^{-1}$ ,  $T_2 = 100^\circ\text{C}$ ,  $T_1 = 20^\circ\text{C}$ , and  $r = 2256 \text{ kJ kg}^{-1}$ .

### 1.4 Cavitation bubble energy

The energy of a spherical cavitation bubble is

$$E_B = \frac{4\pi}{3}(p_0 - p_v)R_{\max}^3, \quad (3)$$

where  $R_{\max}$  is the radius at the time of maximum bubble expansion,  $p_0$  is the hydrostatic pressure, and  $p_v$  the vapor pressure inside the bubble ( $p_v = 2330 \text{ Pa}$  at  $20^\circ\text{C}$  and  $p_0 = 0.1 \text{ MPa}$  [19]). The bubble size is related to its oscillation period  $T_B$  by the Rayleigh equation [20]

$$R_{\max} = \frac{T_B}{2 \times 0.915 \sqrt{\frac{\rho_0}{p_0 - p_v}}}. \quad (4)$$

The oscillation period was determined through a hydrophone measurement of the acoustic transients emitted upon optical breakdown and bubble collapse [21]. It was confirmed in preliminary measurements [22] that (4), which was derived for spherical bubbles, gives good results also for elongated bubbles arising after fs breakdown (the error was less than 3% for bubbles with a ratio of 5:1 between long and short axis). In that case,  $R_{\max}$  corresponds to the radius of a sphere having the same volume as the elongated bubble.

### 1.5 Acoustic energy

The shock wave energy is given by [23]

$$E_S = \frac{4\pi r_m^2}{\rho_0 c_0} \int p^2 dt, \quad (5)$$

where  $r_m$  denotes the distance from the emission center at which the pressure  $p$  is measured. Use of (5) for a determination of the total acoustic energy requires knowledge of the shock wave profile  $p(t)$  in the immediate vicinity of the laser plasma, because further away a large part of the shock wave energy is already dissipated [11, 24]. The shock wave profile close to the plasma is difficult to measure and was therefore obtained through numerical calculations based on the Gilmore model of cavitation bubble evolution [11]. The calculations were performed for a distance  $r_m/R_0 = 6$  from the emission center ( $R_0$  is the plasma radius). Here the shock wave has already acquired the typical form with a steep shock front and an exponential tail, and  $r_m$  is large enough compared to the shock wave width to be approximated by a single value as done in (5). Experimental parameters entering the calculations were the photographically determined plasma volume, the maximum radius of the cavitation bubble, and the laser pulse duration. The shock wave energy obtained this way with the help of (5) is denoted  $E_S^{\text{Gilmore}}$ .

In an alternative approach we evaluated the energy dissipation  $E_{\text{Diss}}$  at the shock front as a function of propagation distance and obtained the shock wave energy by integration over the dissipated energy [24]. The Rankine–Hugoniot equation relates the increase of internal energy per unit mass at a shock front to the change of pressure ( $p_0 \rightarrow p_s$ ) and density ( $\rho_0 \rightarrow \rho_s$ ) at the shock front [25]:

$$\begin{aligned} \Delta\varepsilon(r) &= \frac{1}{2} \left( \frac{1}{\rho_0} - \frac{1}{\rho_s(r)} \right) (p_s(r) + p_0) \\ &\approx \frac{1}{2} \left( \frac{1}{\rho_0} - \frac{1}{\rho_s(r)} \right) p_s(r). \end{aligned} \quad (6)$$

The pressure  $p_s$  and density  $\rho_s$  behind the shock front can be determined through a measurement of the shock front velocity  $u_s$ . The pressure is related to  $u_s$  by [11]

$$p_s = c_1 \rho_0 u_s \left( 10^{(u_s - c_0)/c_2} - 1 \right) + p_0, \quad (7)$$

where  $c_0$  denotes the sound velocity in water,  $c_1 = 5190$  m/s, and  $c_2 = 25\,306$  m/s. The density is, through conservation of mass [25],

$$u_s \rho_0 = (u_s - u_p) \rho_s \quad (8)$$

and momentum [25]

$$p_s - p_0 = u_s u_p \rho_0, \quad (9)$$

also linked with  $u_s$  by [24]

$$\rho_s = \frac{\rho_0}{1 - \frac{p_s}{u_s^2 \rho_0}}. \quad (10)$$

The total change of internal energy during propagation of a spherical shock front from  $r_0$  to  $r_1$  is obtained by integration of (6)

$$E_{\text{Diss}} = \int_{r_0}^{r_1} 4\pi r^2 \rho_s(r) \Delta \varepsilon(r) dr. \quad (11)$$

If measurement data for  $u_s$  are available up to a distance which is at least 10–20 times larger than the plasma radius, (11) can be used for a lower estimate of the shock wave energy, because a major part of the shock wave energy is already dissipated close to the laser plasma [11]. We measured the shock wave velocity  $u_s$  up to a distance of 300  $\mu\text{m}$  from the plasma by taking series of photographs with an increasing time interval between the optical breakdown and the exposure of the photograph [11]. For larger distances the difference  $(u_s - c_0)$  becomes very small, which results in a large measurement uncertainty for  $p_s$  and  $\rho_s$  and thus also for  $E_{\text{Diss}}$ .

To achieve a more complete account of the acoustic energy, we additionally determined the energy  $E_{S/10\text{ mm}}$  remaining at 10 mm distance from the source. For that purpose, the shock wave profile was measured using a PVDF needle hydrophone (Ceram) with a rise time of 12 ns [11].  $E_{S/10\text{ mm}}$  was calculated from the pressure profile by means of (5). The total amount of acoustic energy was then estimated by adding  $E_{\text{Diss}}$  and  $E_{S/10\text{ mm}}$ . The resulting value is still a lower estimate of the acoustic energy, because the dissipation in the range  $0.3\text{ mm} < r < 10\text{ mm}$  is not considered.

### 1.6 Energy of plasma radiation

Barnes and Rieckhoff [26] and Stolarski et al. [27] found that the spectral energy density of the plasma radiation in the wavelength range  $300\text{ nm} < \lambda < 900\text{ nm}$  closely resembles the spectral distribution of a blackbody radiator. The radiant energy emitted by the blackbody depends on its temperature  $T$ , the surface area  $A$  and the duration  $\tau_R$  of the radiation [28]:

$$E_R = \sigma A \tau_R T^4 \quad (12)$$

with the Stefan–Boltzmann constant  $\sigma = 5.670 \times 10^{-8}\text{ W m}^{-2}\text{ K}^{-4}$ . The temperature  $T$  of the blackbody can be determined from the maximum of the spectral distribution  $\rho(\nu)$  using Wien's displacement law

$$T = 1.70 \times 10^{-9} \nu_{\text{max}}. \quad (13)$$

Equation(12) yields an upper estimate of the energy  $E_R$  of the plasma radiation for a given temperature, because it assumes a perfect blackbody radiator. More refined models considering the emissivity  $\varepsilon(\nu)$  of the plasma ( $0 \leq \varepsilon \leq 1$ ) as a function of pressure and temperature of the plasma constituents and of the plasma size have been developed by Weyl and Tucker [29], and by Roberts et al. [30]. However, the simpler approach of (12) suffices already to show that the plasma radiation plays only a minor role in the energy balance of optical breakdown (see below). Data for the plasma temperature determined using (13) were taken from the literature [27], the plasma surface area was determined from plasma photographs, and the duration of the plasma radiation was determined with a fast photodiode (Opto-Electronics AD 110, 380 ps rise time) and oscilloscope (Tektronix 7934, 700 ps rise time). In the case of the ps pulses, where the duration of the plasma radiation was in the order of the response time of the photodiode/oscilloscope system, the measured signal was deconvoluted with the impulse response of the detection system.

## 2 Results and discussion

### 2.1 Complete energy balance for selected parameters

Figure 2 shows the complete energy balance for 6-ns pulses with 1 mJ and 10 mJ energy, and for 30-ps pulses with 50  $\mu\text{J}$  and 1 mJ pulse energy. The lower energy values at each pulse duration are approximately six times above the breakdown threshold, quite typical for the parameter choice in intraocular photodisruption [1, 6]. The common energy value of 1 mJ allows a direct comparison of the energy balance at both pulse durations.

Near threshold, considerably more light is transmitted through the plasma than reflected or scattered. Well above threshold the relative importance of transmission decreases. For all laser parameters, considerably less light is reflected or scattered by the plasma than absorbed. The absorption is thus approximately given by  $A \approx (1 - T)$ . This result differs from the energy partition during plasma formation at solid surfaces where the reflection plays a much larger role, because plasma is formed only within a thin layer in which the electron density tends to exceed the plasma frequency [31] (this is the precondition for a large plasma reflectivity). When plasma is formed in water, however, the breakdown front moves during the rising part of the laser pulse from the beam waist toward the incoming laser beam, because the intensity threshold for breakdown is surpassed ever more upstream [8]. The light absorption by the plasma produced proximal to the laser limits the electron density further downstream, and the plasma frequency remains therefore smaller than the frequency of the laser light. The laser–plasma coupling is thus not impaired, and little light is reflected.

The energy of the plasma radiation  $E_R$  was calculated with the help of (12) and (13). We used the data reported by

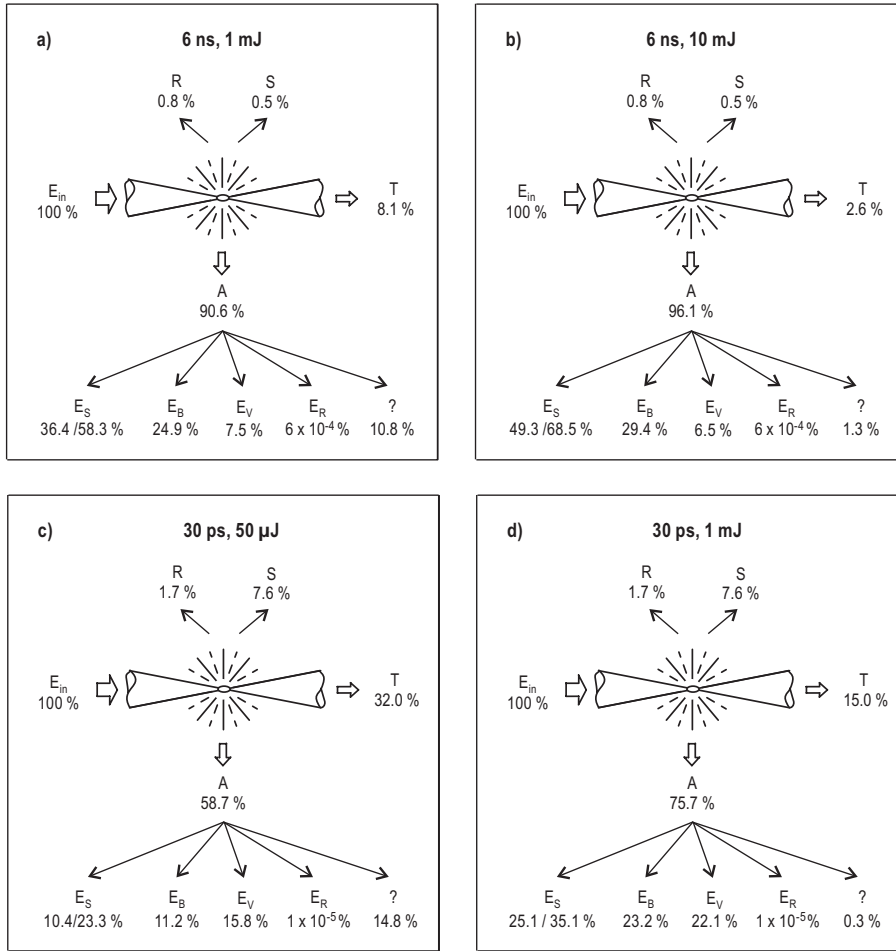


**Fig. 2.** Energy balance for selected laser parameters.  $\lambda = 1064$  nm,  $\theta = 22^\circ$  for ns pulses and  $14^\circ$  for ps pulses. R, S, T, and A denote plasma reflection, scattering, transmission, and absorption. The absorbed energy is divided into shock wave energy  $E_S$ , bubble energy  $E_B$ , evaporation energy  $E_V$ , and the energy of the plasma radiation  $E_R$ . For the shock wave energy two values  $E_S^{\text{Gilmore}}$  and  $(E_{\text{Diss}} + E_{S/10 \text{ mm}})$  obtained by different methods (see Sect. 1.5) are given for each laser parameter. The difference of the complete energy balance to 100% is denoted by “?”. It was calculated using the average of the two energy values quoted for the shock wave energy. All percentages refer to the light energy incident into the laser focus

Stolarski et al. [27] for blackbody temperatures of plasmas produced with Nd:YAG laser pulses at 1064 nm wavelength (9860 K at 5 ns pulse duration and 4 mJ pulse energy; 6230 K at 80 ps pulse duration and 1 mJ pulse energy). The duration of the plasma radiation was measured by us to be 10 ns after a 5-mJ, 6-ns pulse, and 0.5 ns after a 2-mJ, 30-ps pulse. Streak photographic measurements by other authors yielded similar results of 0.24 ns [32] and 0.5 ns [33] for the duration of the plasma radiation. The results of the calculations of  $E_R$  (Fig. 2) demonstrate that the energy loss through plasma radiation is negligible for all laser parameters investigated. This finding agrees qualitatively with the result of previous theoretical investigations of the plasma radiation during laser lithotripsy [29] which showed that the energy carried away by plasma radiation stays below 0.1% of the incident laser light energy during a 1- $\mu$ s laser pulse, when the plasma temperature is 8000 K.

The more relevant pathways for the partition of the absorbed laser energy are evaporation, shock wave generation, and cavitation. Whereas the measurement of the cavitation bubble energy  $E_B$  is fairly straightforward, it is much more difficult to determine the shock wave energy  $E_S$ . The results of the two methods applied to determine the shock wave energy are therefore presented in more detail in Fig. 3 and Table 2.

Figure 3 shows the accumulated energy loss  $E_{\text{Diss}}$  as a function of propagation distance for two laser parameters.

The loss rate is highest close to the plasma and has considerably decreased at the end of the measurement range. A major part of the shock wave energy is, hence, dissipated already within the first 200–300  $\mu$ m from the source. The dissipation amounts to 85%–89% of the total acoustic energy ( $E_{\text{Diss}} + E_{S/10 \text{ mm}}$ ) (Table 2). The shock wave energy is therefore strongly underestimated if it is determined only through far-field measurements as done in earlier studies [34, 35].

The value  $(E_{\text{Diss}} + E_{S/10 \text{ mm}})$  is a lower estimate of the total amount of acoustic energy, because the dissipation in the range  $0.3 \text{ mm} < r < 10 \text{ mm}$  is not considered. The error is, however, small because most of the dissipation occurs already in the region  $r < 0.3 \text{ mm}$  close to the plasma. The error is, furthermore, probably compensated or even overcompensated by the fact that our calculations of  $E_{\text{Diss}}$  do not consider that a part of the acoustic energy deposited as internal energy behind the shock front flows back into the shock wave at its trailing edge [23].

The values for  $E_S^{\text{Gilmore}}$  obtained from calculated pressure profiles by means of (5) are by 28%–55% smaller than  $(E_{\text{Diss}} + E_{S/10 \text{ mm}})$ . A reason for this discrepancy is probably that part of the shock wave energy is already dissipated until the shock wave reaches the location  $r_m/R_0 = 6$  where the pressure profile and  $E_S^{\text{Gilmore}}$  were calculated.

In spite of the differences in absolute values, both methods applied for determining the shock wave energy yield the result that the acoustic energy constitutes the largest in-

**Table 2.** Shock wave parameters and shock wave energies obtained by different methods. The values given for the laser pulse energy refer to the energy incident into the cuvette and the energy absorbed at the laser focus (in brackets)

	30 ps		6 ns	
	50 $\mu$ J (25 $\mu$ J)	1 mJ (0.64 mJ)	1 mJ (0.77 mJ)	10 mJ (8.2 mJ)
<i>Near-field data</i>				
Pressure $p_s$ at plasma rim /MPa	1300	1700	2400	7150
Dissipated energy $E_{\text{Diss}}/\mu\text{J}$	8.4	250	450	5200
<i>Shock wave parameters at <math>r = 10</math> mm</i>				
Pressure $p_s$ /MPa	0.24	1.06	0.99	2.62
Duration $\tau_s$ /ns	43	70	77	148
Energy $E_{S/10\text{ mm}}/\mu\text{J}$	1.5	48	46.2	622
<i>Measured shock wave energy</i>				
$E_{\text{Diss}} + E_{S/10\text{ mm}}/\mu\text{J}$	9.9	298	496	5822
Conversion of absorbed energy into shock wave energy ( $E_{\text{Diss}} + E_{S/10\text{ mm}})/\%$	39.6	46.6	64.4	71.0
<i>Calculated shock wave energy at <math>r_m/R_0 = 6</math> (from [13])</i>				
$E_S^{\text{Gilmore}}/\mu\text{J}$	4.44	214	309	4190
Conversion of absorbed energy into shock wave energy $E_S^{\text{Gilmore}}/\%$	17.8	33.4	40.1	51.1

dividual amount in the energy balance of optical breakdown. The ratio of shock wave energy to cavitation bubble energy was  $\approx 1.5:1$  for ps pulses and  $\approx 2:1$  for ns pulses (Fig. 2). For calculation of these ratios we used the average of the shock wave energies obtained by both methods.

For all laser parameters investigated, a much larger part of the incident light energy was transformed into mechanical energy ( $E_S + E_B$ ) than into evaporation energy (Fig. 2). This feature is particularly pronounced with the 6-ns pulses where the mechanical energy is on average 12 times larger than the evaporation energy; with the 30-ps pulses it is about 2 times

as large. The high conversion efficiency of light energy into mechanical energy is the cause for the disruptive character of plasma-mediated laser surgery [10, 14].

The difference of the complete energy balance to 100% was on average  $-6.8\%$ , and at maximum  $-14.8\%$  (with 50- $\mu$ J, 30-ps pulses). Considering the measurement uncertainties of the individual parts of the energy balance, which is particularly large for the shock wave energy, this result is very satisfactory. One possible explanation for the deficit is that the light lost by scattering in sideward direction was not taken into account. Furthermore, the amount of thermally dissipated energy may have been underestimated. We considered only the energy required to transform the liquid in the breakdown volume into vapor of  $100^\circ\text{C}$ , neglecting losses by heat conduction. Losses by heat conduction are most important for the 50- $\mu$ J, 30-ps pulse, where the largest deficit to 100% was observed, because the penetration depth of heat diffusion ( $1\text{--}2\ \mu\text{m}$ , see Sect. 1.3) is here not very much smaller than the photographically determined plasma radius ( $8.5\ \mu\text{m}$ ). For the other laser parameters, the radius of a sphere of equivalent size to the plasma volume ranges between  $18\ \mu\text{m}$  for the 1-mJ, 6-ns pulse,  $26\ \mu\text{m}$  for the 1-mJ, 30-ps pulse, and  $37\ \mu\text{m}$  for the 10-mJ, 6-ns pulse. In these cases, heat conduction by  $1\text{--}2\ \mu\text{m}$  hardly enlarges the evaporated liquid volume.

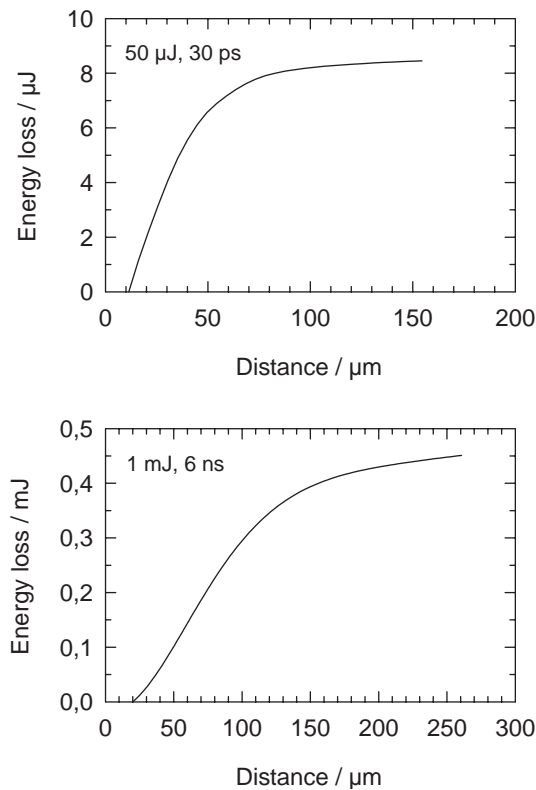


**Fig. 3.** Accumulated energy loss  $E_{\text{Diss}}$  at the shock front vs. propagation distance  $r$  for two laser parameters

## 2.2 Parameter dependence of energy deposition

The parameter dependence of the energy deposition at the optical breakdown site can be derived from the parameter dependence of plasma transmission, because the complete energy balance for selected parameters showed that the plasma absorption is approximately given by  $A \approx (1 - T)$ . Figure 4 presents transmission data  $T(E/E_{\text{th}})$  for different focusing angles, and Fig. 5 shows the transmission as a function of laser pulse duration.

**2.2.1 Dependence on focusing angle.** Figure 4 demonstrates that the plasma transmission increases with decreasing focusing angle. This finding is quite surprising at first sight, because a decreasing focusing angle goes along with an approximately quadratic increase of the plasma length when the

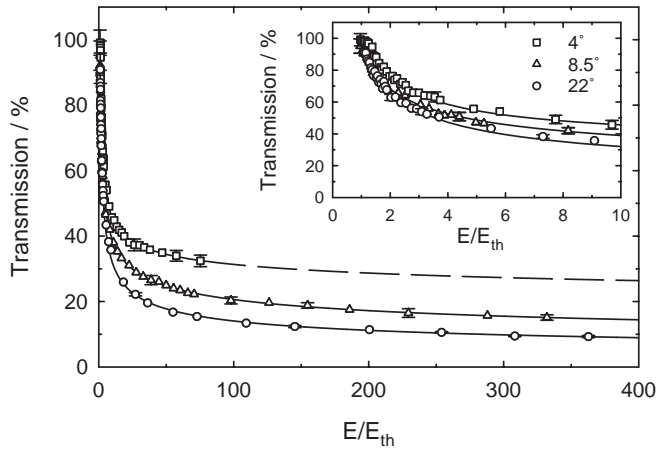


**Fig. 4.** Plasma transmission at various focusing angles, plotted as a function of the normalized laser pulse energy  $\beta = E/E_{th}$ . Pulse duration 30 ps, wavelength 1064 nm

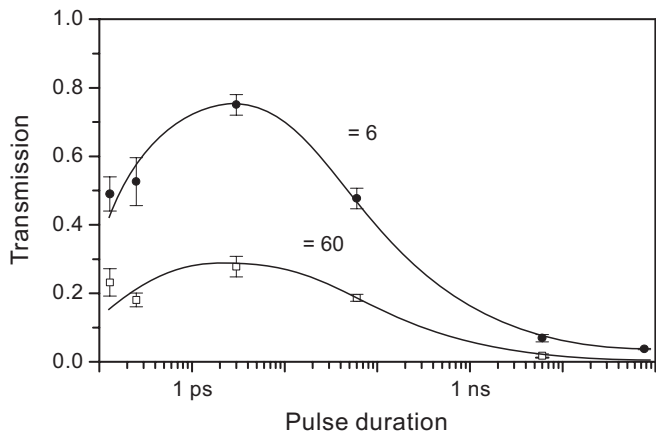


**Fig. 5.** Plasma transmission as a function of laser pulse duration for  $\beta = 6$  and  $\beta = 60$ . The measured data points are connected with lines to facilitate orientation

dimensionless pulse energy  $\beta = E/E_{th}$  is kept constant [8]. The increase of transmission can only be understood, if the increased plasma length is compensated for by a decrease of the absorption coefficient in the plasma. This is indeed the case, because the energy density of the plasma decreases with smaller focusing angle: at a certain energy, the plasma can grow into the cone of the laser beam until it reaches the cross section for which  $I = I_{th}$ . This cross section is the same regardless of the focusing angle, but the distance between laser focus and the cross section is larger for smaller angles. Therefore, the volume of the cone is larger and the energy density less for smaller angles. This results in a smaller rate for inverse bremsstrahlung absorption events, because this rate depends on the free-electron concentration and on the collision frequency between electrons and heavy particles which both decrease with decreasing plasma energy density [16, 36].

**2.2.2 Dependence on pulse duration.** Figure 5 shows that the transmission strongly depends on the laser pulse duration  $\tau$ . It is small in the ns range, but considerably larger for ps pulses, with a maximum around 3 ps. In the fs range, the transmission decreases again. Two factors contribute to the observed  $T(\tau)$  dependence. (i) ns plasmas are, at equal  $\beta$  and equal focusing angle, considerably longer than ps and fs plasmas [8,

22]. Therefore, they absorb more light at equal absorption coefficient. (ii) The time evolution of the free-electron concentration during the laser pulse changes with pulse duration [22, 37, 38]: With ns pulses the electron concentration reaches high values already early in the pulse which leads to a large value of the average absorption coefficient. With ps pulses the maximum is achieved much later during the pulse. That leads to a decrease of the average absorption coefficient. With fs pulses a high electron density is again reached earlier due to the increasing role of multiphoton ionization. This explains the increase of absorption (decrease of transmission) for fs pulses.

The experimentally observed pulse-duration dependence of energy deposition might be influenced by the fact that the data for 6-ns and 76-ns pulse duration were collected at wavelengths of 1064 nm and 750 nm, respectively, whereas the data for shorter pulse durations were collected at 532 nm and 580 nm (see Table 1). Previous transmission measurements [16] performed at 1064 nm and 532 nm with 6-ns and 30-ps pulses showed that the transmission is slightly higher for the shorter wavelength. It was, however, also found that the influence of pulse duration is much stronger than that of wavelength. We can therefore conclude that the trends observed in Fig. 5 would be very similar if all measurements were performed at the same wavelength.

### 2.3 Parameter dependence of conversion of light energy into mechanical energy

In Sect. 2.1 the division of mechanical energy into shock wave energy and cavitation bubble energy was found to be largely independent of the laser parameters: The ratio  $E_S/E_B$  was always between 1.5:1 and 2:1 for laser parameters ranging from 50  $\mu$ J pulse energy at 30 ps duration to 10 mJ at 6 ns. The easily measurable bubble energy can therefore be used as a ‘marker’ for the total mechanical energy to elucidate the parameter dependence of the conversion of light energy into mechanical energy.

**2.3.1 Dependence on focusing angle.** Figure 6 shows that the conversion efficiency of light energy into cavitation bubble

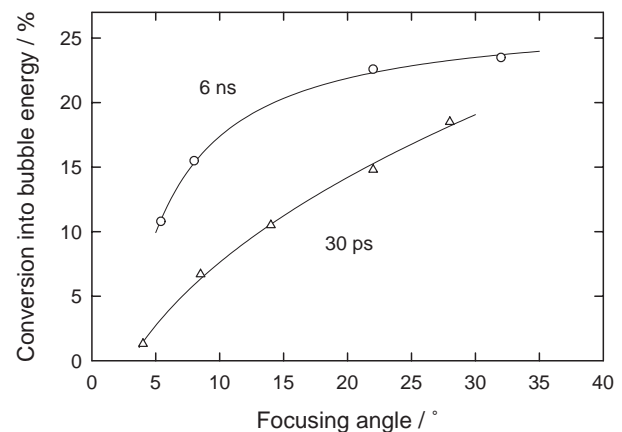


**Fig. 6.** Conversion efficiency of incident light energy into cavitation bubble energy as a function of focusing angle  $\theta$ , for energies well above the breakdown threshold ( $\beta > 10$ )

energy increases with increasing focusing angle. The conversion efficiency depends on the focusing angle, because the energy density in the plasma volume increases with larger focusing angles, as explained already in Sect. 2.2. With a larger energy density, a smaller percentage of the laser energy is required for the evaporation of the liquid in the plasma volume, and a larger fraction is available for the generation of mechanical effects.

**2.3.2 Dependence on pulse duration.** The conversion efficiency into bubble energy was always smaller for 30-ps pulses than for 6-ns pulses, regardless of the focusing angle (Fig. 6). Figure 7 shows that the conversion efficiency decreases even more when the pulse duration is reduced into the fs range. This trend is caused by the decrease of the radiant energy threshold  $F_{th}$  with decreasing pulse duration

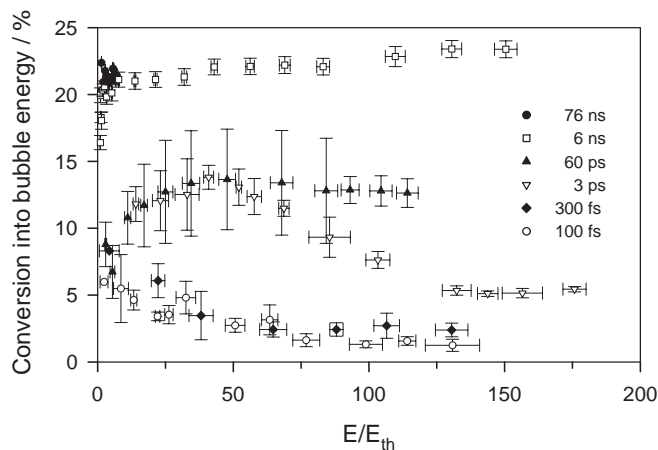


**Fig. 7.** Conversion efficiency of absorbed light energy into cavitation bubble energy as a function of the normalized laser pulse energy  $\beta = E/E_{th}$  for various laser pulse durations

(Table 1). The decrease of  $F_{th}$ , in turn, leads to a decrease of the average energy density in the breakdown region. Experimentally we found the energy density to be 30–40 kJ/cm<sup>3</sup> for ns pulses [11] and less than 1 kJ/cm<sup>3</sup> for 100-fs pulses [15]. These values were obtained by comparing the absorbed laser energy with the volume of the breakdown region determined from photographs.

The pulse-duration dependence of energy density can be explained by looking at the dynamics of energy deposition during breakdown [22, 28, 37]. The absorbed optical energy first produces free electrons, and in a second step the electron energy is transferred by collisions and recombination to the molecules (or dissociated atoms) in the breakdown region. The energy transfer time is in the order of a few ps [39]. With ns pulses, the pulse duration is much longer than the energy transfer time, and therefore a temperature equilibrium between free electrons and heavy particles is achieved during the pulse. Because the equilibrium temperature approximately equals the temperature of the free electrons, it corresponds to a large energy density in the breakdown volume. With fs pulses, however, very little energy has at the end of the laser pulse been transferred to the heavy particles. An equilibrium temperature develops only after the laser pulse. It will be considerably lower than in the case of ns pulses, because the specific heat of the electrons is much smaller than that of the molecules and atoms [39]. Due to the low equilibrium temperature, the energy density in the fs plasmas is much smaller than in the ns plasmas.

An additional factor explaining the small conversion of light energy into bubble energy with fs pulses is heating of the liquid upstream of the actual breakdown zone where a bubble is produced [22, 37]. This phenomenon was observed by laser flash photography in conjunction with a Schlieren technique (Fig. 8). The energy used for heating of the liquid adjacent to the bubble is, of course, lost for the bubble generation and expansion itself. Similar observations have not been made for ns

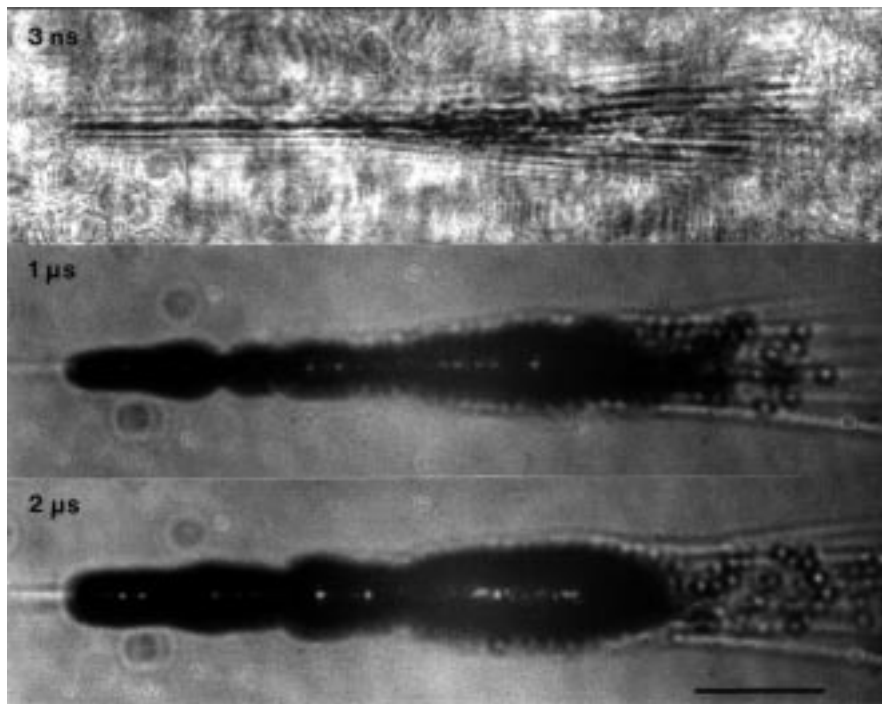


**Fig. 8.** Optical breakdown region after a 100-fs pulse with 35  $\mu\text{J}$  energy ( $\beta = 200$ ), photographed at different times after breakdown using laser flash photography with exposure times of 5 ps (*top*) and 200 ns (*middle* and *bottom*) [15, 22]. The pictures taken 1 and 2  $\mu\text{s}$  after breakdown are slightly defocused to visualize zones of elevated temperature outside the cavitation bubble (shadow method [40]). The laser light was incident from the right, the bar represents a length of 100  $\mu\text{m}$

or ps pulses [22, 37]. The free electron density  $\rho_e$  produced by ns and ps pulses increases very sharply when the peak irradiance is raised from values below the breakdown threshold to values above threshold [38]. The strong  $\rho_e(I)$  dependence corresponds to a sharp border of the breakdown region, which is defined by an iso-intensity surface with  $I = I_{th}$ . With fs pulses, a considerable electron density is reached already at irradiance values slightly below the breakdown threshold, due to the large role of multiphoton absorption, and the  $\rho_e(I)$  dependence is weaker [38]. Therefore, the border of the zone into which the laser energy is deposited is less well defined than with longer pulses.

**2.3.3 Dependence on pulse energy.** At pulse durations of 3 ps or shorter, the conversion efficiency of absorbed light energy into bubble energy reaches a maximum at small values of the normalized pulse energy  $\beta$ , and decreases again at energies well above threshold (Fig. 7). The decrease of conversion efficiency at large  $\beta$  values reflects a decrease of the energy density in the breakdown volume which can be understood as follows: For ps and fs pulses, the plasma length varies approximately proportional to  $(\beta - 1)^{1/2}$  [8, 22], and the plasma volume is, hence, proportional to  $(\beta - 1)^{3/2}$ . The energy density in the plasma can therefore be written as

$$W = \frac{AE_{in}}{V} \propto \frac{A\beta E_{th}}{(\beta - 1)^{3/2}} \approx \frac{AE_{th}}{\sqrt{\beta}} \quad \text{for } \beta \gg 1. \quad (14)$$

At large  $\beta$  values, the coupling coefficient  $A \approx (1 - T)$  of laser energy into the plasma is approximately constant, because the transmission changes only very slowly (Fig. 4). It can be concluded from (14) that under these circumstances the average energy density decreases with increasing  $\beta$ . For ns pulses, the plasma length is at large focusing angles approximately proportional to  $(\beta - 1)^{1/3}$  [8], and therefore the energy density is, according to (14), independent of  $\beta$ .

For fs pulses, another factor might also contribute to the energy dependence of the conversion efficiency into bubble energy: We observed that the relative size of the zone in front of the breakdown region where the liquid is heated but no bubble is formed (see Fig. 8) increases with increasing  $\beta$  [22, 37]. Therefore, a smaller fraction of absorbed energy is available for bubble formation at large  $\beta$  values.

#### 2.4 Practical consequences

The high conversion efficiency of light energy into mechanical energy is the cause for the disruptive character of plasma-mediated laser surgery and of micromachining inside transparent materials. If nevertheless laser effects with little mechanical side effects are desired, laser parameters must be selected for which the ratio of mechanical energy  $E_{mech}$  to evaporation energy  $E_V$  is as small as possible. Figure 6 indicates that  $(E_{mech}/E_V)$  decreases at small focusing angles, because less light energy is converted into mechanical energy. This is, however, of no real advantage for achieving precise and fine laser effects, because a smaller focusing angle leads to a higher energy threshold for breakdown and a larger volume of the breakdown region. A better strategy for reducing the disruptive character of breakdown is the use of ultrashort laser pulses. It was already demonstrated in Sect. 2.1

that  $(E_{mech}/E_V)$  decreases from  $\approx 12:1$  for 6-ns pulses to  $\approx 2:1$  for 30-ps pulses. It can be deduced from the data in Figs. 4 and 7 that for shorter pulse durations  $(E_{mech}/E_V)$  decreases even further. We assume that the shock wave energy is about twice the bubble energy (as observed for longer pulse durations). The evaporation energy is calculated assuming  $E_V = E_{abs} - E_{mech}$ , and  $E_{abs} = E_{in}(1 - T)$ . This approach differs from the determination of  $E_V$  described in Sect. 1.3, because for fs pulses the border of the breakdown region is not clearly defined at the side of the incoming laser beam (see Fig. 8), and therefore the size of the breakdown volume is uncertain. We obtain a ratio  $(E_{mech}/E_V) \approx 1:2$  for 100-fs pulses at  $\beta = 6$ . Besides the reduction of the energy threshold with decreasing pulse duration, it is the change of energy partition  $E_{mech}/E_V$  from 12:1 for ns pulses to 1:2 for fs pulses that makes it possible to diminish disruptive side effects by use of ultrashort laser pulses. Possible applications are, for example, in the field of refractive corneal surgery. Femtosecond pulses have been used to cut a lenticule into the corneal stroma which was then mechanically removed through a small incision to correct myopia with minimal damage to the outer corneal layers [41].

### 3 Conclusions

The conversion efficiency of light energy into mechanical energy during optical breakdown is larger than with any other laser-material interaction [42–44] – it reaches up to 90% at 6 ns pulse duration (Fig. 2). The effective conversion of light energy into mechanical energy is the cause of the disruptive character of plasma-mediated laser-material interaction in a liquid environment.

At large focusing angles, short and highly absorbing plasmas are achieved, which allow a well localized energy deposition at a low breakdown threshold. Large focusing angles are, however, also associated with a high conversion efficiency into mechanical energy and therefore with a large potential for mechanically induced side effects. The mechanical effects can be dramatically diminished by shortening the laser pulse duration. A reduction of the pulse duration from 6 ns to 100 fs is accompanied by a decrease of  $(E_{mech}/E_V)$  from 12:1 to 1:2. At the same time, the efficiency of energy deposition decreases from  $> 90\%$  to  $\approx 50\%$  (at  $\beta = 6$ ), but this decrease imposes no severe practical limitations on the applicability of fs pulses.

*Acknowledgements.* This work was supported by the German Science Foundation (#Bi321/2-4), The United States Air Force Office of Scientific Research (#2312AAAL014), and TASC (#J06829S95135).

### References

1. A. Vogel: *Phys. Med. Biol.* **42**, 895 (1997)
2. P.K. Kennedy, D.X. Hammer, B.A. Rockwell: *Prog. Quantum Electron.* **21**, 155 (1997)
3. A.A. Oraevsky, L.B. DaSilva, A.M. Rubenchik, M.D. Feit, M.E. Glin-sky, M.D. Perry, B.M. Mammini, W. Small IV, B.C. Stuart: *IEEE J. Sel. Top. Quantum Electron.* **2**(4), 801 (1996)
4. J. Neev, L.B. Da Silva, M.D. Feit, M.D. Perry, A.M. Rubenchik, B.C. Stuart: *IEEE J. Sel. Top. Quantum Electron.* **2**(4), 790 (1996)

5. B.N. Chichkov, C. Momma, S. Nolte, F. von Alvensleben, A. Tünnermann: *Appl. Phys. A* **63**, 109 (1996)
6. R.F. Steinert, C.A. Puliafito: *The Nd:YAG Laser in Ophthalmology* (Saunders, Philadelphia 1985)
7. X. Liu, D. Du, G. Mourou: *IEEE J. Quantum Electron.* **QE-33**, 1706 (1997)
8. A. Vogel, K. Nahen, D. Theisen, J. Noack: *IEEE J. Sel. Top. Quantum Electron.* **2**(4), 847 (1996)
9. P.K. Kennedy, S.A. Boppart, D.X. Hammer, B.A. Rockwell, G.D. Noojin, W.P. Roach: *IEEE J. Quantum Electron.* **QE-31**, 2250 (1995)
10. A. Vogel, P. Schweiger, A. Frieser, M.N. Asiyov, R. Birngruber: *IEEE J. Quantum Electron.* **QE-26**, 2240 (1990)
11. A. Vogel, S. Busch, U. Parlitz: *J. Acoust. Soc. Am.* **100**, 148 (1996)
12. G. Geerling, J. Roeder, U. Schmidt-Erfurt, K. Nahen, E.-S. El-Hifnawi, H. Laqua, A. Vogel: *Br. J. Ophthalmol.* **82**, 504 (1998)
13. F. Docchio, L. Dossi, C.A. Sacchi: *Lasers Life Sci.* **1**, 87 (1986)
14. A. Vogel, M.R.C. Capon, M.N. Asiyov-Vogel, R. Birngruber: *Invest. Ophthalmol. Vis. Sci.* **35**, 3033 (1994)
15. J. Noack, D.X. Hammer, G.D. Noojin, B.A. Rockwell, A. Vogel: *J. Appl. Phys.* **83**, 7488 (1998)
16. K. Nahen, A. Vogel: *IEEE J. Sel. Top. Quantum Electron.* **2**(4), 861 (1996)
17. S. Fujikawa, T. Akamatsu: *J. Fluid Mech.* **97**, 481 (1980)
18. A.J. Welch, M.J.C. van Gemert (Eds): *Optical-Thermal Response of Laser-Irradiated Tissue* (Plenum Press, New York 1995)
19. R.C. Weast (Ed): *CRC Handbook of Chemistry and Physics* (CRC Press, Boca Raton 1988)
20. R.T. Knapp, J.W. Daily, F.G. Hammit: *Cavitation* (McGraw-Hill, New York 1971)
21. A. Vogel, W. Hentschel, J. Holzfuß, W. Lauterborn: *Ophthalmology* **93**, 1259 (1986)
22. J. Noack: Ph.D. Thesis (Medical University of Lübeck, Lübeck, Germany 1998) (in German)
23. R.H. Cole: *Underwater Explosions* (Princeton University Press, Princeton 1948)
24. A. Vogel, J. Noack: *SPIE Proc.* **3254**, 180 (1998)
25. G.E. Duvall, G.R. Fowles: In *High Pressure Physics and Chemistry* ed. by R.S. Bradley (Academic Press, New York 1963) pp. 209–291
26. P.A. Barnes, K.E. Rieckhoff: *Appl. Phys. Lett.* **13**, 282 (1968)
27. D.J. Stolarski, J. Hardman, C.G. Bramlette, G.D. Noojin, R.J. Thomas, B.A. Rockwell, W.P. Roach: *SPIE Proc.* **2391**, 100 (1995)
28. D. Sliney, M. Wolbarsht: *Safety with Lasers and Other Optical Sources* (Plenum Press, New York 1980)
29. G. Weyl, T. Tucker: *Lasers Life Sci.* **3**, 125 (1989)
30. R.M. Roberts, J.A. Cook, R.L. Rogers, A.M. Gleeson, T.A. Griffy: *J. Acoust. Soc. Am.* **99**, 3465 (1996)
31. R.P. Godwin, C.G.M. van Kessel, J.N. Olsen, P. Sachsenmaier, R. Sigel: *Z. Naturforsch. A* **32**, 1100 (1977)
32. F. Docchio: *Europhys. Lett.* **6**, 407 (1988)
33. R.J. Thomas, D.X. Hammer, G.D. Noojin, D.J. Stolarski, B.A. Rockwell, W.P. Roach: *SPIE Proc.* **2681**, 402 (1996)
34. V.S. Teslenko: *Sov. J. Quantum Electron.* **7**, 981 (1977)
35. A. Vogel, W. Lauterborn: *J. Acoust. Soc. Am.* **84**, 719 (1988)
36. Y.R. Shen: *The Principles of Nonlinear Optics* (Wiley, New York 1984)
37. A. Vogel, J. Noack, K. Nahen, D. Theisen, R. Birngruber, D.X. Hammer, G.D. Noojin, B.A. Rockwell: *SPIE Proc.* **3255**, 34 (1998)
38. J. Noack, A. Vogel: submitted to *IEEE J. Quantum Electron.*
39. S. Nolte, C. Momma, H. Jacobs, A. Tünnermann, B.N. Chikov, B. Well-gehausen, H. Welling: *J. Opt. Soc. Am. B* **14**, 2716 (1997)
40. W. Merzkirch: *Flow Visualization* (Academic Press, New York 1974)
41. R.M. Kurtz, C. Horvath, H.H. Liu, T. Juhasz: *SPIE Proc.* **3255**, 56 (1998)
42. V.S. Teslenko: *Sov. J. Quantum Electron.* **7**, 981 (1977)
43. L.M. Lyamshev: *Sov. Phys. Usp.* **24**, 977 (1981)
44. E.J. Chapyak, R.P. Godwin, A. Vogel: *SPIE Proc.* **2975**, 335 (1997)